PHASE-RESOLVED INFRARED *H*- AND *K*-BAND SPECTROSCOPY OF EF ERIDANI[1]

Thomas E. Harrison[2]

Astronomy Department, New Mexico State University, Las Cruces, NM 88003; tharriso@nmsu.edu

Steve B. Howell[3]

WIYN Observatory and National Optical Astronomy Observatory, 950 North Cherry Avenue, Tucson, AZ 85719; howell@noao.edu

Paula Szkody

Department of Astronomy, University of Washington, Box 351580, Seattle, WA 98195; szkody@alicar.astro.washington.edu

Derek Homeier

Department of Physics and Astronomy, University of Georgia, Athens, GA 30602-2451; derek@physast.uga.edu

AND

Joni J. Johnson and Heather L. Osborne

Astronomy Department, New Mexico State University, Las Cruces, NM 88003; jojohnso@nmsu.edu, hosborne@nmsu.edu

Received 2004 May 3; accepted 2004 June 28

ABSTRACT

We present new phase-resolved *H*- and *K*-band spectroscopy of the ultrashort-period magnetic cataclysmic variable EF Eri in its current prolonged "low" state obtained using NIRI on Gemini North and NIRSPEC on Keck II. These new data show that the *H*-band spectrum of EF Eri appears to be dominated by cyclotron emission during the entire orbital cycle. The *K*-band spectrum of EF Eri is likewise dominated by cyclotron emission during most of an orbital period, but near binary phase 0.0 the secondary star spectrum may be visible. The lack of strong CO or CH_4 absorption features and the weakness of the water vapor features in this spectrum, however, suggests the possibility of peculiar abundances for carbon and/or oxygen. We have used the PHOENIX stellar atmosphere code to produce model brown dwarf spectra with nonsolar abundances of carbon, nitrogen, and oxygen, and achieved limited success in fitting the observed spectra. We conclude that strong, highly variable cyclotron emission is responsible for the photometric variation previously reported for EF Eri. The nature of this cyclotron emission is complex: the *H*-band spectra show that the dominant cyclotron harmonic at phase 0.5 peaks at 1.65 μm, but at phase 0.0 the harmonic peaks near 1.72 μm. At phase 0.5, there is another cyclotron feature present that peaks in between the *H* and *K* bands (near 1.93 μm), but at phase 0.0 no such feature is present. These data suggest that cyclotron emission from both poles is occurring. In the high state, the cyclotron emission has been modeled as coming from the pole that is oriented toward the secondary star. One interpretation for the phase 0.5 cyclotron emission is that it originates from the opposite pole. In its current ultralow state, EF Eri reveals no outward signs of accretion (such as H I emission) but continues to have a few, strong cyclotron features. Thus, EF Eri joins the small group of magnetic cataclysmic variables whose accretion rate is so low that they are in the "bombardment scenario" regime.

Subject headings: binaries: close — stars: general — stars: individual (EF Eridani) —
stars: low-mass, brown dwarfs — stars: magnetic fields

1. INTRODUCTION

Polars are magnetic cataclysmic variables (CVs) that have white dwarf primaries with strong magnetic fields that dramatically affect the accretion flow from their cool Roche lobe–filling companions. Instead of forming a disk, the accreted matter flows in a stream from near the L1 point to one or both of the magnetic poles of the white dwarf primary (see Wickramasinghe & Ferrario 2000 for a complete review). For reasons not yet identified, the normal "high state" mass transfer rate ($\approx 10^{-11}$ $M_\odot$ yr^{-1}) ceases and the system transitions to a "low state." For the most extreme examples, accretion rates as low as 10^{-13} $M_\odot$ yr^{-1} or lower have been inferred (Reimers et al. 1999; Schwope et al. 1999; Szkody et al. 2003). When in these low states, polars should present an excellent opportunity to examine the very low mass secondary stars of the shortest period CVs.

EF Eri is an ultrashort-period ($P_{\rm orb} = 81$ minutes) polar that entered a low state in 1997. Harrison et al. (2003) presented simultaneous multiwavelength optical and infrared photometry for EF Eri in its low state in which they believed they had detected the irradiated brown dwarf–like secondary star of this system. Their data showed that in the *BVRIJ* bandpasses, the light curves were dominated by emission from the white dwarf and some residual cyclotron emission, while in the *H* and *K* bands the light curves exhibited large amplitude ($\Delta K = 0.8$ mag) variations that repeated once per orbital cycle. Harrison et al. were able to model these multiwavelength data with an extremely cool ($T_{\rm eff} \leq 1000$ K) secondary star that is being irradiated by the primary. In this model, the irradiated hemisphere of the secondary star is heated to $T_{\rm eff} \approx 1500$ K. If

this model were correct, then the spectroscopic appearance of the secondary star should show dramatic changes over an orbital cycle, oscillating between a state where CO absorption is strong, as in the L dwarfs, to one where methane might dominate, as seen in T dwarfs. We have obtained new phase-resolved *H*- and *K*-band spectra of EF Eri using NIRSPEC on KECK II and *K*-band spectra using NIRI on Gemini-North to test the irradiated brown dwarf model.

2. OBSERVATIONS

EF Eri was observed continuously from 7:21 until 9:00 UT on 2002 December 24 using NIRI[4] on Gemini-North in queue-scheduled mode. For these observations the F/6 camera, a four-pixel slit, and the *K*-grism were used to produce *K*-band spectra with a resolution of $R \approx 780$. Individual spectra, with exposure times of 120 s, were obtained at five different positions along the slit. After each exposure, the telescope was offset by 6″ along the slit, and a new exposure started. In this way, 42 individual spectra were obtained in 100 minutes, covering 123% of an orbital cycle for EF Eri. In addition to this set of continuous spectra, four additional spectra were obtained in the period between 6:10 and 6:19 UT.

To remove telluric features in the spectra of EF Eri, the G2 V star HD 16358 was observed using an identical procedure, but with exposure times of 5 s. At the time of the observation, HD 16358 had an air mass of 1.44, which is very close to the mean air mass attained by EF Eri during the 100 minute observation period. The resulting data set was reduced using a procedure common for reducing infrared spectral data, in which the images are grouped into sets of five individual exposures. A median of four of these exposures is subtracted from the spectrum of interest to remove the sky contamination. A spectrum is then extracted from this sky-subtracted image using the normal LONGSLIT spectroscopic reduction packages within IRAF, and the process is repeated. Each individual spectrum was wavelength calibrated using the spectrum of an argon lamp obtained shortly before our observations began. The wavelength-calibrated spectra of EF Eri were then divided by the median of the five wavelength-calibrated spectra of HD 16358 to remove telluric absorption features. The latter procedure introduces spurious features into the spectra of interest because of weak atomic and molecular absorption lines in the G2 V spectrum. To remove these weak features, we have employed the procedure described by Maiolino et al. (1996).

With only a single standard to work with, the telluric correction for the entire data set is not as good as can be produced (see Harrison et al. 2004) when a large number of such spectra are available. This is evidenced by dips at 2.0 and 2.05 μm in the NIRI spectra presented below. The flux calibration of these data was fairly good, and our spectra revealed the same large amplitude ($\Delta K = 0.8$ mag) flux variations as reported by Harrison et al. (2003). We have assumed that EF Eri has not changed its photometric behavior between the time of the last photometric data set (see below) and the epoch of these observations, allowing us to use the *K*-band light curve to produce flux-calibrated spectra.

EF Eri was observed using NIRSPEC[5] on Keck II on 2003 September 6. We used NIRSPEC in low-resolution mode with the 0″38 slit. We employed the four-nod script to obtain spectra
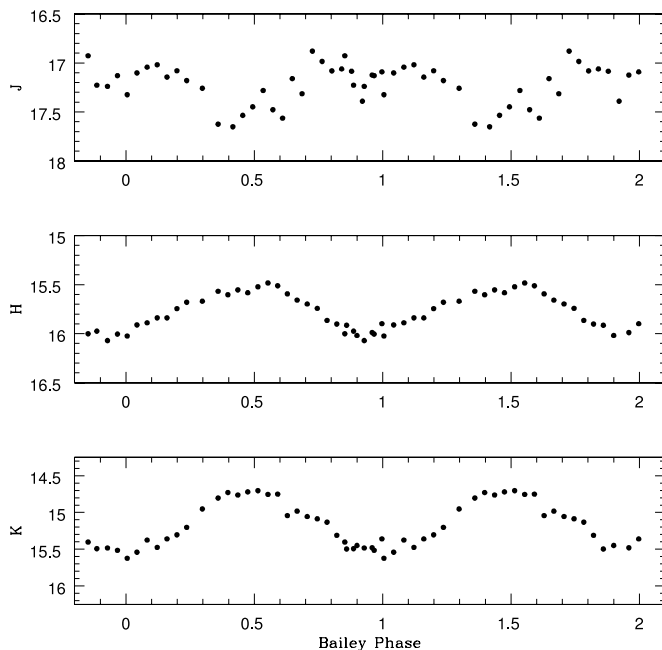
FIG. 1.—Infrared light curves of EF Eri obtained with SQIID on the KPNO 2.1 m. The absolute fluxes and light-curve amplitudes have not changed when compared with those presented in Harrison et al. (2003). The data sets have been plotted over two orbital cycles for clarity.

at four different positions along the slit. For the *H*-band spectra, the grating tilt was set to cover the wavelength range 1.54–1.83 μm with a dispersion of 2.91 Å pixel^{-1}. The *K*-band setup covered the wavelength range 2.00–2.42 μm, with a dispersion of 4.27 Å pixel^{-1}. Because of the strong curvature of the spectra produced by NIRSPEC, each spectrum has a slightly different wavelength coverage that depends on the position of the object along the slit. This effect is apparent in some of the NIRSPEC spectral sequences presented below. The *H*-band data were obtained from 12:29 to 13:57 UT, covering 109% of an orbital cycle. The *K*-band spectra were obtained in the interval 14:24 to 15:25 UT, and covered 88% of an orbital period. HD 16358 was used as the telluric standard for both bandpasses. While the conditions were photometric, we found that the nodding routine did not reliably place our targets exactly on the slit during the four-position nod, and thus we were unable to extract photometric information from these data. We have decided to use the infrared light curves to produce flux-calibrated spectra.

Three months before the Gemini observations, on 2002 September 24, we were able to obtain additional, simultaneous *JHK* photometry of EF Eri using SQIID on the KPNO 2.1 m. These data were reduced in the same fashion as our earlier observations (see Harrison et al. 2003 for full details). The conditions during this run were poorer than those of our 2001 run, and the *J*-band light curve (see Fig. 1) has a lower signal-to-noise ratio (S/N) than the earlier effort. The *H*- and *K*-band data, however, reveal identical light curves to the 2001 data set, showing no evidence for changes in either the absolute flux levels or the amplitude of the variations.

Harrison et al. (2003) found that the phasing of EF Eri by Bailey et al. (1982), where phase 0 corresponded to the appearance of a sharp dip in the *J*-band light curve, appeared to be identical to the binary orbital phase. We have used the same set of ephemerides to phase the data here. Because of EF Eri's extremely short period, the spectral smearing caused by the orbital motion is significant. We have used the evolution code
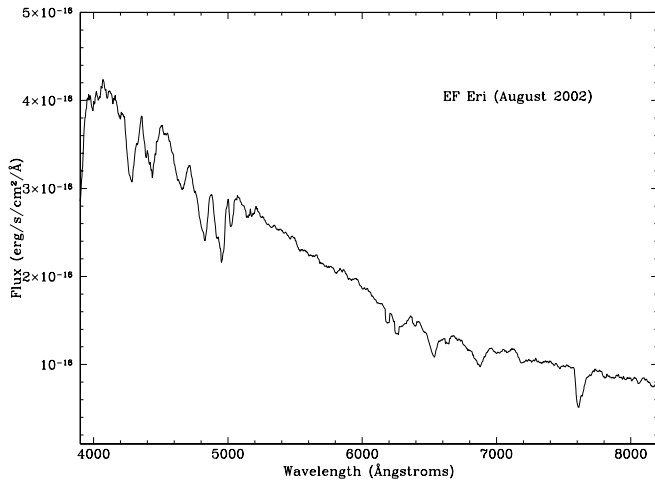
Fig. 2.—Optical spectrum of EF Eri obtained with EMMI on NTT on 2002 August 10. The accretion rate in EF Eri has declined to the point where there is no longer detectable emission at Hα. The $\sigma^{\pm}$ features from the Zeeman splitting of the H I lines, however, are clearly seen. The central, unshifted absorption components of H I are weaker than expected, suggesting the possibility of continued low-level emission.

predictions by Howell et al. (2001) to estimate the masses of the two components in the EF Eri system as $M_1 = 0.6\ M_{\odot}$ and $M_2 = 0.06\ M_{\odot}$. Using an orbital inclination of $45°$ (see Harrison et al. 2003 and references therein), we estimate the radial velocity semiamplitude of the secondary in EF Eri to be $K_2 = 340$ km s^{-1}. The full orbital variation corresponds to only about two resolution elements in the NIRI spectra, but six resolution elements for the Keck spectra. Thus, to allow us to co-add the individual spectra to search for features from the secondary star, we have Doppler corrected our data using this estimated value for K_2.

In our ongoing program of continued occasional monitoring EF Eri, we have obtained a new optical spectrum using the EMMI[6] spectrograph in the red imaging low dispersion (RILD) mode on the New Technology Telescope (NTT). This spectrum, shown in Figure 2, was obtained on 2002 August 10, is a 600 s exposure, and has a resolution of 2.3 Å. It is interesting to compare this spectrum with those presented in Harrison et al. (2003) and Beuermann et al. (2000): the Zeeman absorption features are now more pronounced, and the emission from H I has continued to decline to the point where it is no longer detectable.

3. RESULTS

In the preceding section we noted that we have produced flux-calibrated spectra by using the infrared light curves for EF Eri. We did this so as to produce a consistent set of data that would enable us to ignore slit losses in either set of spectra. Comparison of data sets obtained on widely separated epochs such as those analyzed here could be compromised by intrinsic variations in EF Eri. While we are confident about the photometric "stability" of EF Eri up to and including the Gemini data, there is no assurance that EF Eri was in the same state when we observed it with Keck. But to make sense of the Gemini NIRI data we were required to assume that the *H*-band spectra obtained with NIRSPEC represents a similar state in EF
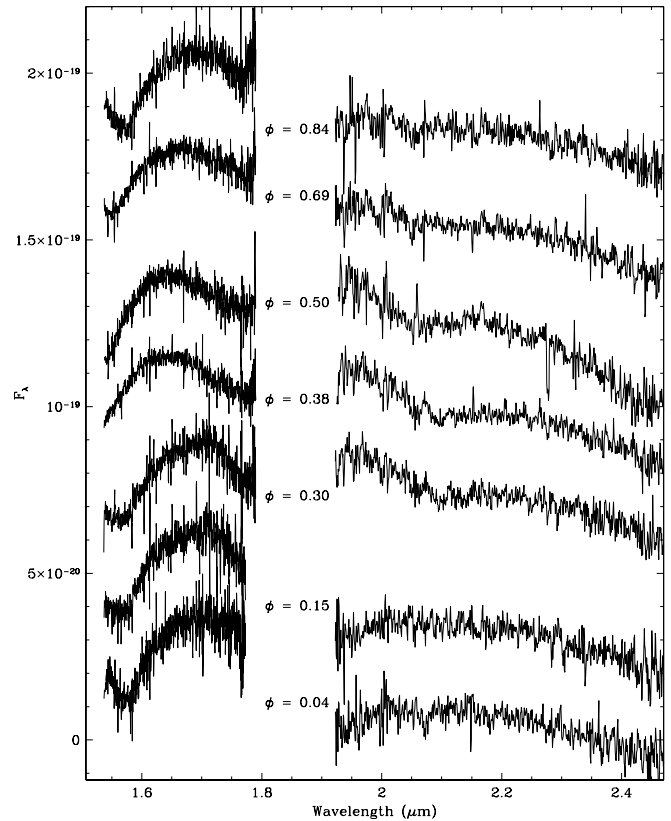
6 More information on EMMI is available at http://www.ls.eso.org/lasilla/Telescopes/NEWNT/emmi.

Fig. 3.—Keck NIRSPEC *H*-band spectra and Gemini NIRI *K*-band spectra of EF Eri. Both data sets have been flux calibrated using the infrared light curves. For clarity, the *H*- and *K*-band spectra for each orbital phase have been offset in flux. The mean orbital phases of the spectra are listed.

Eri. The fact that the NIRSPEC *K*-band data had similar phase-dependent morphology gives us confidence in this assumption.

In Figure 3 we present the *H*- and *K*-band spectra for EF Eri at a number of orbital phases. Each of these spectra is the median of four (*H*) or five (*K*) individual spectra. The *H*-band spectra in this plot have been produced as described above. The telluric correction scheme of Maiolino et al. (1996) truncates the blue end of the *K* band at 1.94 μm. Because of the blueward rise seen in the NIRI spectra of EF Eri, we have also reduced the *K*-band spectra by simple raw division of these data by the telluric standard and then multiplied the divided spectra by the spectrum of the appropriate blackbody. This allowed us to extend our wavelength coverage down to $\approx$1.92 μm. This latter method, however, introduces weak "emission" features from the G-star division (see Fig. 1 in Harrison et al. 2004). Given the low S/N of our data set, the only obvious such feature is the false H I Brγ emission line at 2.16 μm visible in the spectra with orbital phases near 0.5.

3.1. *The H-Band Spectra*

During one orbital cycle, the *H*-band spectra undergo remarkable changes. Near phase 0.0 (i.e., minimum light), the spectra show a pronounced blueward rise. Note that the data have relatively high S/Ns in this region, since it is not near the blue cutoff of the *H* band. Alternatively, one could suggest that there is a single, broad absorption feature located at 1.574 μm. After this dip, the spectrum rises to a broad maximum whose peak is near 1.72 μm. As we show below, this is not the expected behavior for the spectrum of a normal late-type/brown dwarf star.
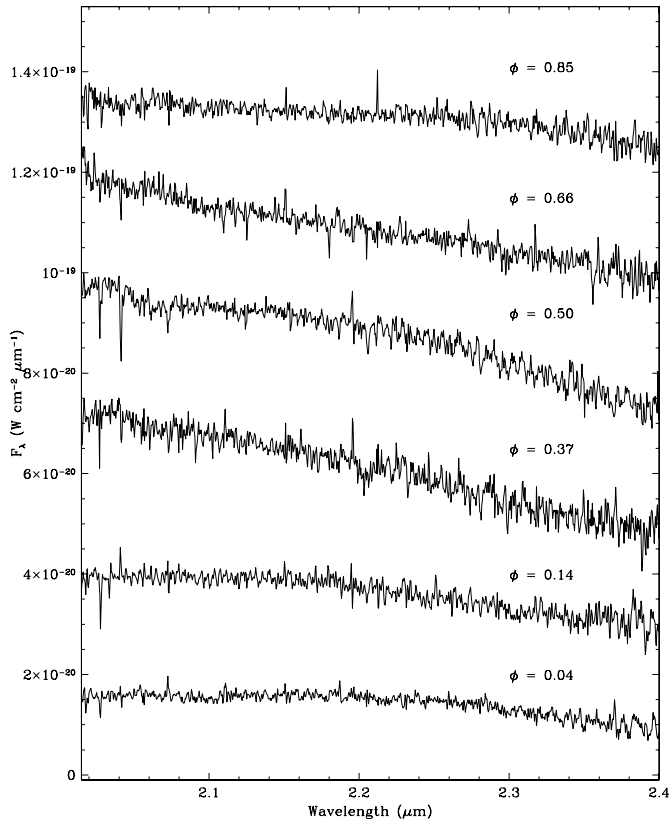
FIG. 4.—NIRSPEC K-band phase-resolved spectra of EF Eri. These data have been flux calibrated using the infrared light curves and then offset for clarity. The same phase-dependent morphology seen in the Gemini data set is present here. Each spectrum is the median of several 3 minute exposures.

As the orbital phase progresses from phase 0.0, the blue-ward rise rapidly disappears and the flux peak in the spectrum moves to the blue. It is unclear whether this blue feature completely disappears or is simply hidden by the much higher flux levels associated with the phase 0.5 cyclotron emission. During the transition to maximum light, a weak rise at the extreme red end of the H band appears. While the S/N of the data in this region is quite low, the combination of the H- and K-band data sets suggest that this rise is real and is due to a broad feature that peaks somewhere between the edges of the H and K bandpasses, in the middle of the region strongly affected by telluric water vapor absorption. As the orbital phase continues to increase on its way back to phase 0.0, the spectra retrace their premaximum evolution.

3.2. The K-Band Spectra

The K-band spectra obtained with NIRI are shown in Figure 3, and the K-band spectra obtained with NIRSPEC are presented in Figure 4. Both data sets show similar evolution over an or-bital cycle, suggesting that little has changed in the intervening nine months. Near phase 0.0, the spectrum shows a continuum that is consistent with that of a late-type star, with declining fluxes at both blue and red ends, which is presumably caused by water vapor absorption in the photosphere of the secondary star. The co-addition of the NIRSPEC phase 0.0 spectra (Fig. 5) do not confirm this, however, with no clear sign of the expected spectral features for a late-type star. *This is true even when we correct the spectra for the predicted radial velocity of the secondary star.* While a feature consistent with $^{12}CO_{(2,0)}$ (at 2.294 μm) appears to be present, other features with a similar
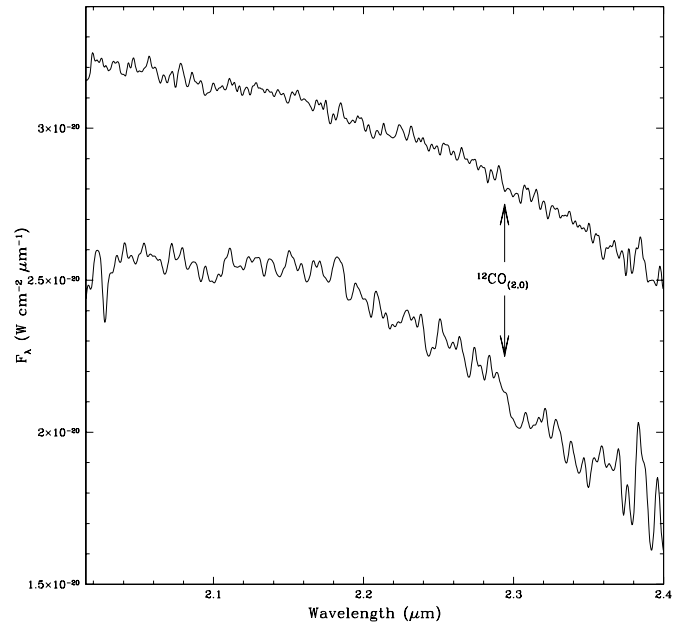

FIG. 5.—Median of the entire NIRSPEC K-band data set (*top line*, offset in flux), and a smoothed (to FWHM = 60 Å) median of the seven spectra closest to phase 0.0 (*bottom line*). A possible very weak absorption feature at the position of the first overtone of $^{12}CO_{(2,0)}$ (at 2.294 μm) is seen in both spectra, and appears to be the only indication of the presence of the secondary star besides the decline at the red end of the K band that might be associated with water vapor absorption.

depth do not correspond to any of the expected atomic features (e.g., Na I at 2.20 μm) for a cool star. By co-adding the entire NIRSPEC data set, the first overtone feature of $^{12}CO_{(2,0)}$ appears to remain marginally detectable. This would be the first detec-tion of the secondary star in EF Eri.

As the orbital phase advances, the spectra show rapid changes, with the development of a pronounced hump blue-ward of 2.10 μm and an increasingly steeper continuum be-yond 2.2 μm. This blue hump is better defined in the NIRI spectra because of their extended blue coverage. Note that the telluric water vapor absorption below 2.0 μm is very strong, and thus the shape of the continuum here is highly sensitive to the telluric correction. While the blueward rise begins well before this difficulty, the exact form of the slope of the continuum below 2.0 μm is not well defined with the current data set.

3.3. The Secondary Star of EF Eri

As we have just noted (see Fig. 5), combining the entire NIRSPEC data set has allowed us to tentatively detect the secondary star in EF Eri. While the S/Ns of these data are not high, if the secondary star were relatively normal it should be more prominent than seen here. By modeling the optical spectrum of EF Eri, Beuermann et al. (2000) have derived distances for EF Eri in the range $80 \le d \le 128$ pc, while Thorstensen (2003) has measured a distance of 163 ± 58 pc via parallax. Thorstensen finds that an astrometric solution with a distance of 113 pc is possible by adjusting some of the input criteria. As shown in Harrison et al. (2003), the optical photometry of EF Eri is well modeled by a 9500 K white dwarf, and this white dwarf provides no more than 10% of the flux in the K band. If we assume that the secondary star is responsible for the remainder of the K-band flux at phase 0.0 ($K = 15.55$), the absolute magnitude of EF Eri is in the range $10.0 \le M_K \le 11.0$. This absolute magnitude corresponds to a
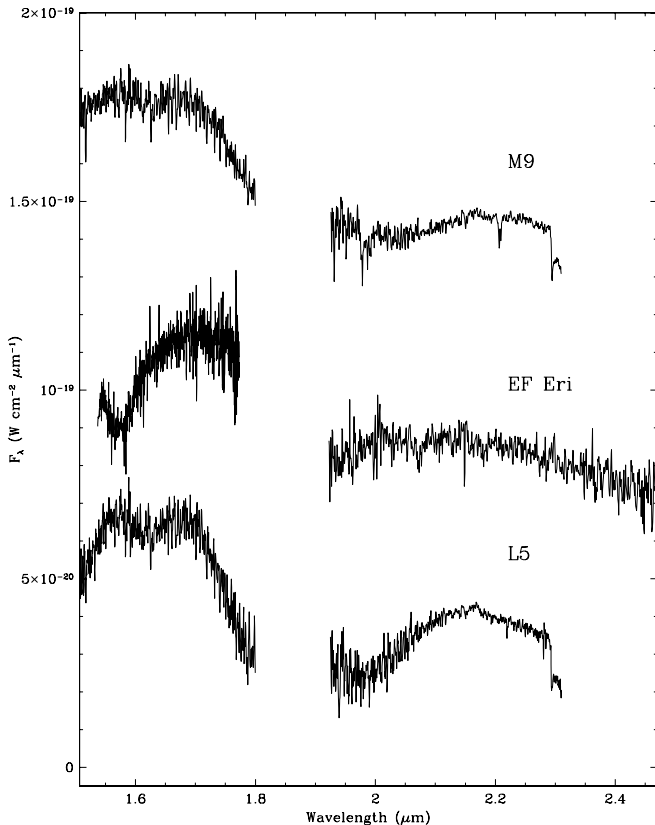
Fig. 6.—Comparison of the phase 0.0 spectrum of EF Eri with those of M9 and L5 dwarfs (from McLean et al. 2003). The sharp feature at 2.294 μm in the comparison spectra is due to the first overtone feature of CO.

vapor features in those objects appear to be relatively normal, Harrison et al. suspect that carbon is deficient in those systems. This view is supported by the analysis of far-ultraviolet (FUV) observations of CVs by Gänsicke et al. (2003), in which large N v/C iv ratios have been found, suggesting nitrogen enhancements and carbon deficits in the photospheres of the white dwarf primaries, presumably arising from matter transferred from the secondary star. It would therefore not be unexpected for the secondary star in EF Eri to have anomalously weak CO absorption features. A lowered carbon abundance would also reduce the CH_4 absorption expected for late-L and T dwarfs, and thus could produce much redder $J - K$ colors through the range of possible spectral types for the secondary of EF Eri.

To test this hypothesis we have calculated theoretical spectra using the general stellar atmosphere code PHOENIX (Hauschildt et al. 1999) for a variety of chemical compositions that might be expected in a CNO-processed stellar core. Depth-dependent partial pressures for more than 650 species are calculated using the equation of state (EOS) of Allard & Hauschildt (1995) by solving chemical equilibrium for 40 elements, as described in Allard et al. (2001), including dust formation. Model structures and flux spectra are computed self-consistently, treating line blanketing by the direct opacity-sampling method, with line strengths taken from a master database of 43 million atomic and 700 million molecular lines. In addition, dust extinction profiles for 31 grain species are included. Major updates relative to the AMES-Cond and AMES-Dusty models of Allard et al. (2001) are the addition of 30 million methane lines from D. Homeier et al. (2004, in preparation), and the explicit treatment of the gravitational settling of dust grains developed by Allard et al. (2003). In addition, the Ames list of water line opacities from Partridge & Schwenke (1997) has been replaced by the earlier list from Miller et al. (1994) for these models. The latter list is less complete for high-temperature steam, but has been found to give better agreement with the IR spectra of cool brown dwarfs (D. Homeier et al. 2004, in preparation). Nevertheless, we emphasize that none of the currently available databases for molecular opacities accurately reproduces the observed shape of all absorption bands in the IR. These models also suffer from incomplete or missing data for several molecules, such as CrH and FeH. For example, the *H*-band spectra of mid-L dwarfs show a moderately strong absorption feature near 1.6 μm (see Fig. 6) that is not reproduced by any of our models. Several features in this region have been identified by Cushing et al. (2003) with the $E^4\Pi-A^4\Pi$ system of FeH, for which no line opacity data are available at this time. Possibly because of this missing opacity source and other uncertainties in input data such as H_2O opacities and dust extinction profiles, our theoretical spectra tend to produce $H - K$ colors that are too blue when compared to observed L dwarfs (Legget et al. 2001).

We have constructed grids of models based on revised solar abundances as compiled by Lodders (2003), except for carbon, oxygen and nitrogen, which were altered as indicated for the individual models. The basic atmospheric parameters span the range 1400 K $\leq T_{eff} \leq$ 2500 K, and log $g = (4.5, 5.0, 5.5)$. First, investigating the effects of lowering the carbon abundance to $[C/Fe] = (-0.5, -1.0, -1.5)$, we find that a depletion to at least 0.1 times solar is required to explain the weakness or absence of the CO overtone bands. From synthetic photometry, we can also exclude models with T_{eff} significantly higher than 2000 K, since these disagree with the observed J magnitudes, even assuming the upper limit of 5.5 for the distance modulus. Below 1600 K, the strong methane bands at 2.2–2.3 μm

spectral type in the range M8 to L1 (ignoring any effects due to the Roche lobe–filling nature of this object).

A secondary star with a spectral type near M9 should have strong CO features, as well as a detectable Na i doublet. We have compared the combined *H*- and *K*-band spectra of EF Eri with published spectra for stars and brown dwarfs in the range M7 V to T8. While the overall slope of the continuum of the phase 0.0 *K*-band spectrum is consistent with a very late–type M dwarf (see Fig. 6), the *H*-band spectrum bears no resemblance to such an object. The departure becomes more pronounced when we compare the spectrum of EF Eri to those of L dwarfs. While brown dwarfs around L5 show a similar spectral slope at 1.55–1.6 μm, there is no feature comparable to the strong flux peak at 1.7 μm. While the absence of Na i in the *K* band is consistent with a spectral type later than L0 (McLean et al. 2003), the water vapor absorption bands of such an object are much deeper and depress the blue side of the *K*-band spectrum much farther to the red ($>$2.1 μm) than is seen in EF Eri. Also, the first-overtone CO bandhead at 2.29 μm remains strong in brown dwarfs until CH_4 takes over in the late L types.

In addition to the difference in *H*- and *K*-band spectral features, the *JHK* photometry is almost impossible to reconcile with any known dwarf. While the *H*-band–to–*K*-band flux ratios for EF Eri are more-or-less consistent with those of late-type objects, giving rise to $H - K = 0.42$ ($\approx$M8 V), the observed $J - K$ color ($>$2.5) exceeds even the reddest IR colors observed in mid-L dwarfs (Legget et al. 2001).

3.3.1. *Model Spectra for Carbon/Oxygen-Depleted Atmospheres*

As shown in Harrison et al. (2004), many CV secondary stars show evidence for weak CO absorption features. Since the water
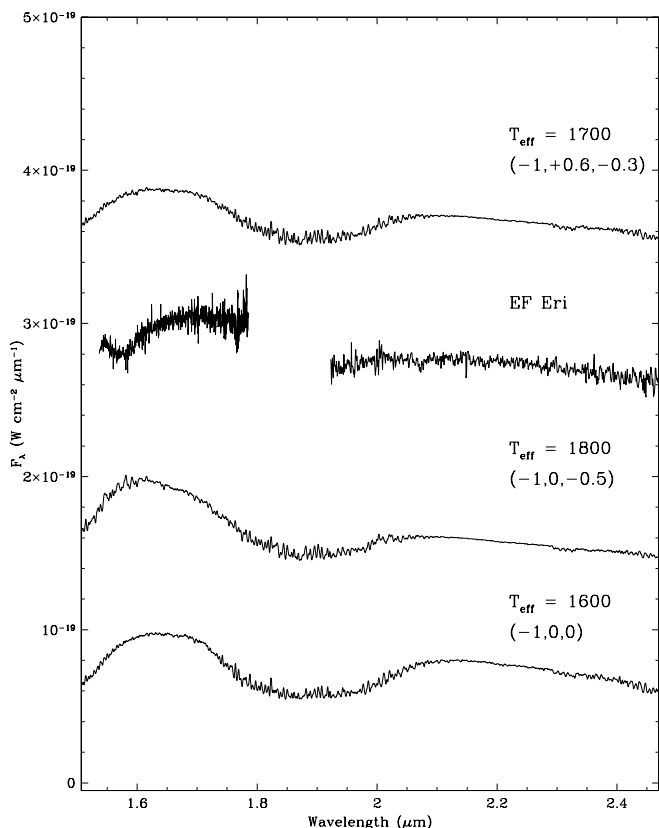
Fig. 7.—Comparison of the phase 0.0 spectrum of EF Eri with brown dwarf model spectra generated using PHOENIX. The temperature of each model is listed, and each of these models has a gravity of $\log g = 5.0$. Below the temperature are the abundances of carbon, nitrogen, and oxygen (in dex, vs. solar). The top model has deficits of carbon and oxygen and enhanced levels of nitrogen ($4 \times$ solar). The bottommost model simply has a carbon deficit ($0.1 \times$ solar). The oxygen-deficient models fit the observed K-band spectrum because of their shallower water vapor absorption. None of the models we developed, however, could explain the shape of the H-band spectrum of EF Eri.

become prominent even at $[C/Fe] = -1.0$, but lowering the carbon abundance farther does not improve the fit to the observed K-band spectrum at such low temperatures. We find the best agreement for the red part of the K-band spectrum for models with $1600 \text{ K} \leq T_{\text{eff}} \leq 1800 \text{ K}$, as shown by the bottom spectrum in Figure 7. However, a carbon deficiency alone cannot explain the early onset of absorption to the blue side of the K band, which appears at much shorter wavelengths than typically seen both in our models and in observations of L dwarfs. Nor can a lack of carbon be responsible for the peculiar shape of the H-band spectra. The main opacity source at these wavelengths is water vapor, and significant changes can only be expected if the oxygen abundance is reduced as well. Such effects might be expected if the secondary CNO cycle has been active for some time, although models by Marks & Sarna (1998) do not indicate significant changes in the oxygen abundance for CNO processed material. We have nonetheless produced test models for $[O/Fe] = -0.5$ to explore this case. As one would expect, these models (Fig. 7) show an onset of the water vapor bands in both the H and K bands at shorter wavelengths, with a K-band spectrum that fits our observations quite well. For comparison, a model with an additionally enhanced nitrogen abundance, as would be expected with the depleted carbon and oxygen transformed into ^{14}N, is also shown.

Synthetic colors calculated for these models show that the nitrogen-enriched atmosphere produces the closest match to the $J - K$ and $H - K$ photometry. We have not attempted to modify our input chemistry further to optimize these fits, since such results would necessarily be of limited significance given the uncertainties in the available opacity data and the limited wavelength coverage of our spectra. Clearly, a direct detection of the water absorption in the H band, which we expect to occur at $1.5–1.55 \mu m$, and J-band spectra would help in resolving these uncertainties. Such data would also allow for the study of irradiation, which is expected to have the strongest impact at shorter wavelengths (Barman et al. 2002). In conclusion, a brown dwarf with a considerable deficiency of carbon, a lesser depletion of oxygen, and an enhancement of nitrogen reproduces much of the secondary's IR spectral energy distribution (SED) and the shape of the K band at phase 0.0. The additional absorption at $1.6 \mu m$ cannot be accounted for in the current models. If this band is indeed due to FeH, we expect it to become relatively stronger when the steam bands are reduced. In that case, the spectra could probably reproduce the "base" of the H-band emission. The shape of the actual peak, however, does not correspond to any known stellar features, and also shows changes with phase that cannot be explained by irradiation effects. We conclude that cyclotron emission at $1.6–1.8 \mu m$ contaminates the infrared spectrum for all orbital phases.

3.4. The Cyclotron Features

It is clear that the H-band spectra are inconsistent with that of a normal (or chemically altered) late-type or brown dwarf secondary star. If the phase 0.0 dip near $1.6 \mu m$ is associated with FeH, then we estimate that $\approx 30\%$ of the H-band flux at this juncture is due to cyclotron emission. Thus, to produce the observed, phase-dependent changes in the H-band spectra probably requires two separate cyclotron features in this bandpass. If we assume the phasing and geometry from Bailey et al. (1982), the phase 0.0 cyclotron features that we see in the H band are presumably associated with the pole that accretes during the high state. This suggests that the single, dominant cyclotron feature at phase 0.5 might be from the other pole.

While the minimum-light K-band spectrum is fairly consistent with the shape of a cool star spectrum, with little evidence for cyclotron emission, the maximum-light spectrum is clearly contaminated by at least one, possibly two cyclotron features. Obviously, there is a cyclotron harmonic that peaks below $2.0 \mu m$. The rapid change in slope of the red half of the K-band spectrum and the dip near $2.07 \mu m$ suggest the possibility of an additional, weaker cyclotron feature at phase 0.5. To better examine the phase 0.5 cyclotron features, we have subtracted the phase 0.0 spectrum from the phase 0.50 spectrum to produce the residual spectrum shown in Figure 8. The result shows two strong cyclotron features, one that peaks in the H band near $1.58 \mu m$ and one that (we estimate) peaks near $1.93 \mu m$. The possibility of a second cyclotron feature in the K band seems more likely after this subtraction. If the secondary star has a similar spectrum at phases 0.0 and 0.5, then any water vapor feature should disappear on subtraction. Ignoring the false H I Brγ emission feature, there continues to be a modest dip near $2.07 \mu m$ and a small rise that peaks near $2.15 \mu m$ and falls off slowly beyond $2.2 \mu m$.

4. DISCUSSION

Regardless of the exact interpretation of the spectra presented here, it is clear that the model proposed by Harrison et al. (2003) is incorrect. The photometric modulations in the
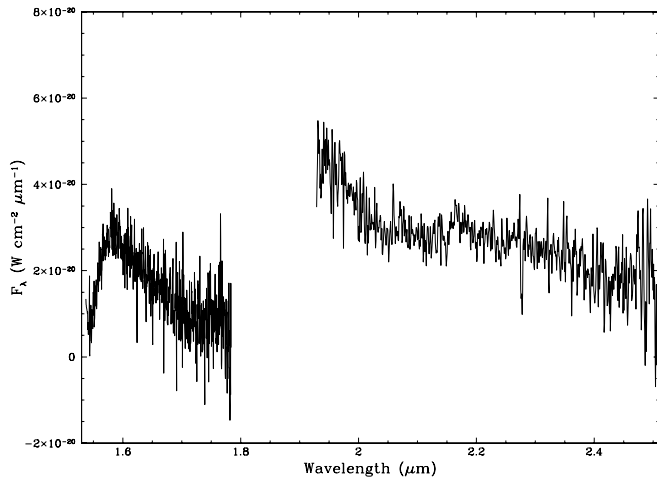
Fig. 8.—Residual spectrum created by subtracting the phase 0.0 spectra from the phase 0.5 spectra. The result is two apparent cyclotron humps that peak near 1.58 and 1.93 μm.

K band are certainly being driven by the changing strength of the cyclotron feature at the blue end of this bandpass (and possibly aided by a broader and weaker feature that peaks near 2.15 μm). There is very little evidence for the secondary star in our *K*-band spectra, with only the suggestion of a weak first overtone CO feature in the median of the *K*-band data set. While the presence of weak CO features in a CV is not surprising (see Harrison et al. 2004), stars with the late spectral type expected for the secondary in EF Eri have *H*-band spectra that are completely different to what we have observed. While model brown dwarf spectra with dramatic alterations in the abundances of the major opacity sources at these wavelengths do a somewhat better job at fitting the data, neither the observations or the models are currently adequate to truly investigate the nature of the underlying secondary star.

The fact that cyclotron emission can still dominate the spectrum of EF Eri in this low state is surprising given that EF Eri exhibits no outward signs of continued accretion. The optical and infrared spectra lack Balmer and Brackett emission from H i. The optical *BVRI* spectral energy distribution and spectrum are completely consistent with that of an inactive magnetic white dwarf. The model white dwarf atmosphere, with $T_{\rm eff} = 9500$ K, used by Harrison et al. (2003) to compare with their 2001 March 11 spectrum of EF Eri, does an excellent job at fitting the 2002 August 10 optical spectrum we obtained with NTT. Clearly, the white dwarf photosphere alone is too cool to supply significant quantities of ionizing photons. It appears that the white dwarfs in ultrashort-period, low mass transfer rate CVs are significantly cooler than those in longer period or higher mass transfer rate systems (cf. Szkody et al. 2002).

Four magnetic CV systems have now been found that display a single, dominant cyclotron feature in their optical spectra that have been attributed to very low mass transfer rates: SDSS J155331.12+551614.5, SDSS J132411.57+032050.5 (Szkody et al. 2003), RBS 0206 (= EQ Cet; Schwope et al. 1999), and HS 1023+3900 (= WX LMi; Reimers et al. 1999). Along with the single very large cyclotron feature is evidence for a second, weaker feature at the next lower/higher harmonic number covered by their optical spectra. Of these four polars, both SDSS J155331.12+551614.5 and J132411.57+032050.5 have optical light curves that resemble the infrared light curves of EF Eri (see Figs. 2 and 6 of Szkody et al. 2003). SDSS 1553 shows optical variations with peak-to-peak amplitudes of

$\Delta m \approx 1$ mag in *V* and *R*, while SDSS 1324 has variations in the Sloan *r*-band of $\Delta r = 1.3$ mag. Both sets of light curves are roughly sinusoidal, similar to the *H*- and *K*-band light curves of EF Eri. Unlike EF Eri, however, the spectra of both SDSS 1553 (Fig. 1 in Szkody et al. 2003) and SDSS 1324 (G. Schmidt 2004, private communication) reveal H i emission.

The interpretation of the spectra of SDSS 1553, SDSS 1324, EQ Cet, and WX LMi is that they have entered phases of extremely low accretion rates, the so-called bombardment solution (Kuijpers & Pringle 1982), where any heating is from particle collisions instead of shocks. This state is characterized by low plasma temperatures, and mass transfer rates of $\dot{M} \leq 10^{-13}$ $M_{\odot}$ yr^{-1}. In each of these four polars, the harmonic numbers of the dominant cyclotron features are in the range $2 \leq n \leq 4$, with magnetic field strengths above 45 MG. Magnetic field strength estimates for EF Eri range from 10 to 21 MG. Assuming $B \sim 14$ MG, the $n = 4$ harmonic would peak at 1.96 μm and the $n = 5$ harmonic would peak at 1.58 μm. The $n = 3$ harmonic would peak near 2.6 μm, while the $n = 6$ and 7 harmonics would appear in the *J* band. It is worth noting that during the *H*- and *K*-band maxima, the *J*-band light curve shows a minimum. Given this fact, and the need for very high accretion rates to produce power in these higher harmonics, it is likely that the $n = 6$ and 7 harmonics are not significant sources of flux in EF Eri. The fact that the *J*-band light curve has a maximum during the *H*- and *K*-band minima suggests activity from another pole with a significantly higher magnetic field strength. The flux peak at 1.72 μm and the upturn at the blue end of the phase 0.0 *H*-band spectra, along with the lack of significant cyclotron emission in the *K* band, indicate that the phase 0.0 cyclotron emission comes from a region with a significantly different field strength. A fit to the cyclotron features of the high state *JHK* spectra of EF Eri by Ferrario et al. (1996) suggested emission from two regions with magnetic field strengths of 16.5 and 21 MG. An accreting pole with a field strength of 21 MG would not produce a cyclotron feature in the *K* band, but would produce harmonics at 1.7 and 1.3 μm, consistent with our phase 0.0 spectra.

That the magnetic field structure of EF Eri is complex, including strong evidence for emission from more than one pole, has been demonstrated by Hutchings et al. (1982), Piirola et al. (1987), Meggit & Wickramasinghe (1989), and Ferrario et al. (1996). Recent "magnetic field topology" mapping of the magnetic field of the white dwarf in EF Eri by Reinsch et al. (2003) reveals this complexity: there are two main polar caps with field strengths as high as 100 MG at their centers, as well as evidence for multiple zonal components. The complex structure of the field in EF Eri must be partly to blame for the results presented here. Modeling the cyclotron features that would arise from accretion onto such a field would be helpful in unraveling our spectroscopic results.

The lack of detectable H i emission from EF Eri when compared with the other members of its small family is interesting. It is highly likely that the current accretion rate in EF Eri is lower than the other four objects and is simply not sufficient to supply the heating necessary to generate the UV photons required to create H i emission. In the bombardment scenario, the accretion shock disappears and the white dwarf photosphere is directly heated by particle collisions. A lower accretion rate means less heating and therefore less ionizing radiation.

The secondary star of EF Eri remains elusive. Beuermann et al. (2000) have presented arguments that the spectral type of the secondary star in EF Eri must be later than M9, with the most probable spectral type later than L3. We can estimate the

maximum amount of flux from the secondary by assuming that the flux level of the dip seen in the phase 0.0 H-band spectrum (at 1.57 μm) represents the continuum level of the underlying secondary star. This corresponds to $H_{sec} \geq 16.5$. Assuming $80 \leq d \leq 128$ pc, the absolute H magnitude of the secondary star is in the range $11.0 \leq M_H \leq 12.0$, consistent with an early/mid-L dwarf. Thus, EF Eri joins WZ Sge (see Howell et al. 2004) as the CVs with the strongest evidence for harboring brown dwarf–like secondary stars.

5. CONCLUSIONS

We have obtained phase-resolved infrared spectroscopy of EF Eri and conclude that the large amplitude variations seen in its infrared light curve are not due to a heated brown dwarf but have their origin in cyclotron emission. EF Eri appears to join the small family of polars in which the accretion rate has dropped to a very low level. Unfortunately, our data are inadequate to allow us unravel the complex cyclotron emission that is present in EF Eri. Phase-resolved J-band spectroscopy is required to make further progress in disentangling the cyclotron spectrum of EF Eri. Given that the mean J-band magnitude of EF Eri is 17.3, multiple orbits of data on 8 m class telescopes will be needed to obtain spectra with sufficient S/Ns. To fully interpret the spectroscopic observations, phase-resolved, broadband JHK polarimetric observations of EF Eri will be essential. It would also be extremely useful to have a radial velocity curve for the EF Eri system to allow us to properly phase and co-add the infrared spectra to search for features from the secondary star. Such data could be acquired through optical spectroscopy of the Zeeman absorption features of H I.

REFERENCES

Allard, F., Guillot, T., Ludwig, H., Hauschildt, P. H., Schweitzer, A., Alexander, D. R., & Ferguson, J. W. 2003, in IAU Symp. 211, Brown Dwarfs, ed. E. Martín (San Francisco: ASP), 325
Allard, F., & Hauschildt, P. H. 1995, ApJ, 445, 433
Allard, F., Hauschildt, P., Alexander, D., Tamanai, A., & Schweitzer, A. 2001, ApJ, 556, 357
Bailey, J., Hough, J. H., Axon, D. J., Gatley, I., Lee, T. J., Szkody, P., Stokes, G., & Berriman, G. 1982, MNRAS, 199, 801
Barman, T. S., Hauschildt, P. H., & Allard, F. 2002, in ASP Conf. Ser. 261, The Physics of Cataclysmic Variables and Related Objects (San Francisco: ASP), 49
Beuermann, K., Wheatley, P., Ramsay, G., Euchner, F., & Gänsicke, B. T. 2000, A&A, 354, L49
Cushing, M. C., Rayner, J. T., Davis, S. P., & Vacca, W. D. 2003, ApJ, 582, 1066
Ferrario, L., Bailey, J., & Wickramasinghe, D. 1996, MNRAS, 282, 218
Gänsicke, B. T., et al. 2003, ApJ, 594, 443
Harrison, T. E., Howell, S. B., Huber, M. E., Osborne, H. L., Holtzman, J. A., Cash, J. L., & Gelino, D. M. 2003, AJ, 125, 2609
Harrison, T. E., Osborne, H. L., & Howell, S. B. 2004, AJ, 127, 3493
Hauschildt, P. H., Allard, F., & Baron, E. 1999, ApJ, 512, 377
Howell, S. B., Harrison, T. E., & Szkody, P. 2004, ApJ, 602, L49
Howell, S. B., Nelson, L. A., & Rappaport, S. 2001, ApJ, 550, 897

Hutchings, J. B., Cowley, A. P., Crampton, D., Fisher, W. A., & Liller, M. H. 1982, ApJ, 252, 690
Kuijpers, J., & Pringle, J. E. 1982, A&A, 114, L4
Leggett, S. K., Allard, F., Geballe, T. R., Hauschildt, P. H., & Schweitzer, A. 2001, ApJ, 548, 908
Lodders, K. 2003, ApJ, 591, 1220
Maiolino, R., Rieke, G. H., & Reike, M. J. 1996, AJ, 111, 537
Marks, P. B., & Sarna, M. J. 1998, MNRAS, 301, 699
McLean, I. S., McGovern, M. R., Burgasser, A. J., Kirkpatrick, J. D., Prato, L., & Kim, S. S. 2003, ApJ, 596, 561
Meggitt, S. M. A., & Wickramasinghe, D. T. 1989, MNRAS, 236, 31
Miller, S., Tennyson, J., Jones, H., & Longmore, A. 1994, in IAU Colloq. 146, Molecular Opacities in the Stellar Environment, ed. P. Thejll & U. G. Jørgensen (New York: Springer), 296
Partridge, H., & Schwenke, D. W. 1997, J. Chem. Phys., 106, 4618
Piirola, V., Reiz, A., & Coyne, G. V. 1987, A&A, 186, 120
Reimers, D., Hagen, H., & Hopp, U. 1999, A&A, 343, 157
Reinsch, K., Euchner, F., & Beuermann, K. 2003, preprint (astro-ph/0302056)
Schwope, A. D., Schwarz, R., & Greiner, J. 1999, A&A, 348, 861
Szkody, P., Gänsicke, B. T., Sion, E. M., & Howell, S. B. 2002, ApJ, 574, 950
Szkody, P., et al. 2003, ApJ, 583, 902
Thorstensen, J. R. 2003, AJ, 126, 3017
Wickramasinghe, D. T., & Ferrario, L. 2000, PASP, 112, 873